# Radio frequency radiation-induced hyperthermia using Si nanoparticle-based sensitizers for mild cancer therapy

Konstantin P. Tamarov, Liubov A. Osminkina, Sergey V. Zinovyev, Ksenia A. Maximova, Julia V. Kargina, Maxim B. Gongalsky, Yury Ryabchikov, Ahmed Al-Kattan, Andrey P. Sviridov, Marc Sentis, et al.

SCIENTIFIC REPORTS

OPEN

SUBJECT AREAS:
NANOTECHNOLOGY IN CANCER
RADIOTHERAPY

Received
6 May 2014

Accepted
24 October 2014

Published
13 November 2014

Correspondence and requests for materials should be addressed to A.V.K. (kabashin@lp3.univ-mrs.fr) or V.Y.T. (timoshen@physics.msu.ru)

# Radio frequency radiation-induced hyperthermia using Si nanoparticle-based sensitizers for mild cancer therapy

Konstantin P. Tamarov[1], Liubov A. Osminkina[1], Sergey V. Zinovyev[2], Ksenia A. Maximova[3], Julia V. Kargina[1], Maxim B. Gongalsky[1], Yury Ryabchikov[3], Ahmed Al-Kattan[3], Andrey P. Sviridov[1], Marc Sentis[3], Andrey V. Ivanov[2], Vladimir N. Nikiforov[1], Andrei V. Kabashin[3] & Victor Yu Timoshenko[1]

[1]Lomonosov Moscow State University, Department of Physics, 119991 Moscow, Russia, [2]Blokhin Russian Cancer Research Center, 115478 Moscow, Russia, [3]Aix Marseille University, CNRS, LP3 UMR 7341, Campus de Luminy - Case 917, 13288, Marseille Cedex 9, France.

**Offering mild, non-invasive and deep cancer therapy modality, radio frequency (RF) radiation-induced hyperthermia lacks for efficient biodegradable RF sensitizers to selectively target cancer cells and thus avoid side effects. Here, we assess crystalline silicon (Si) based nanomaterials as sensitizers for the RF-induced therapy. Using nanoparticles produced by mechanical grinding of porous silicon and ultraclean laser-ablative synthesis, we report efficient RF-induced heating of aqueous suspensions of the nanoparticles to temperatures above 45-50 °C under relatively low nanoparticle concentrations (<1 mg/mL) and RF radiation intensities (1–5 W/cm²). For both types of nanoparticles the heating rate was linearly dependent on nanoparticle concentration, while laser-ablated nanoparticles demonstrated a remarkably higher heating rate than porous silicon-based ones for the whole range of the used concentrations from 0.01 to 0.4 mg/mL. The observed effect is explained by the Joule heating due to the generation of electrical currents at the nanoparticle/water interface. Profiting from the nanoparticle-based hyperthermia, we demonstrate an efficient treatment of Lewis lung carcinoma *in vivo*. Combined with the possibility of involvement of parallel imaging and treatment channels based on unique optical properties of Si-based nanomaterials, the proposed method promises a new landmark in the development of new modalities for mild cancer therapy.**

Cancer remains a major threat to mankind, despite significant progress in the past decade in understanding, treating and preventing the disease. Since about 40% of found tumors are not resectable, they are usually treated by relatively "heavy" chemotherapy methods, which provide average survival for about 1 year even if multiple sequential chemotherapeutic regimes are used[1]. An ability of radio frequency (RF) radiation to heat human tissues is known for a long time, but after recent demonstrations of a local destruction of cancer tumors using invasive RF ablation it attracted renewing interest of scientists[2–4]. The RF ablation method results in successful partial necrosis of tumor, but turns out to be dangerous in many situations as the improvement of blood circulation under RF irradiation can provoke a further development of tumors[3,4], and is applicable only for a few organ sites (liver, kidney, breast, lung, bone)[2–4].

The efficiency of RF-based therapy can be significantly enhanced by using sensitizers, or properly designed absorbing agents, which are targeted into a tumor area (actively or passively), accumulate in it, and then absorb main RF radiation power to heat cancer cells and thus cause their selective destruction as schematically shown in Fig. 1a. Such effect can be achieved by using electrically-conductive nanoparticles (NP's)[5,6]. According to a model proposed by Moran et al[6], such NPs can produce Joule heating through the RF-induced generation of local electrical currents over the NP volume. Gold NPs nanoparticles and carbon nanotubes were selected as candidates for these tasks providing a strong absorption of RF radiation even under relatively small concentrations of NPs of the order of 1 mg/mL[5–8]. In particular, an intense source of the RF radiation with frequency of 13.6 *MHz* and the power of 600 *W* induced the heating of suspensions of gold (Au) NPs with heating rate ~20 K/sec, which resulted in a considerable cell necrosis[6]. *In vivo* experiments with Au NPs, intro-tumoraly injected in rats and irradiated by RF waves at 35 *W* for 13 min, demonstrated a significant temperature increase and a thermal injury of the

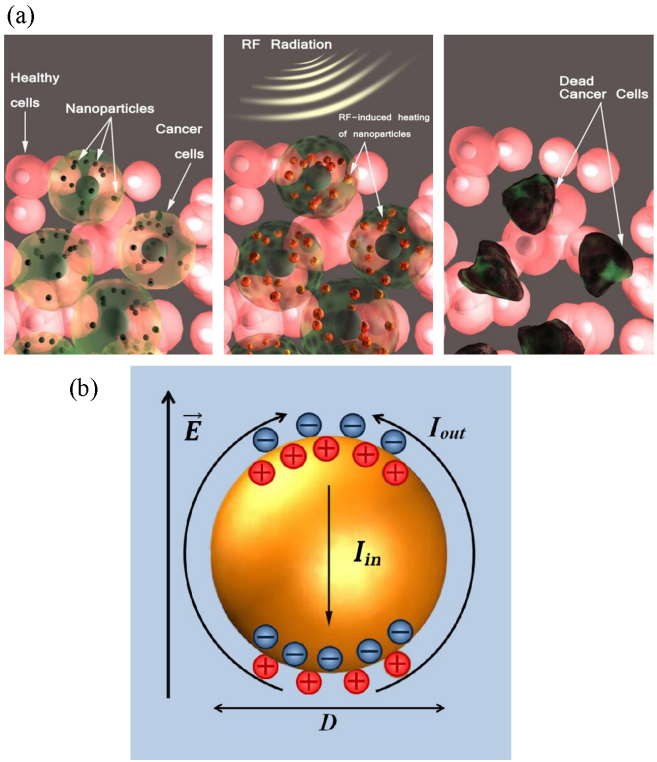


**Figure 1 | Radio frequency (RF) radiation-induced hyperthermia using RF-absorbing Si nanoparticle-based sensitizers.** (a) Schematic representation of the treatment procedure. The nanoparticles are first selectively accumulated in tumor cells through passive or active targeting. Then, they are heated by RF radiation causing a local increase of temperature and selective death of cancer cells, while adjacent tissues remain unaffected, (b) Distribution of electric field around a solid polarizable sphere immersed in a liquid electrolyte (water) during RF irradiation. A dipolar charge cloud is formed due to the ion movement in electrical double layer in response to RF-induced sphere polarization.

hepatoma tumor at injection sites, while the histopathologic assessment of tumor showed a widespread tumor cell disaggregation associated with the nuclear hyperchromatism, cytoplasmic retraction and areas of apoptosis and cell fragmentation[8]. However, there are major concerns in using Au NPs and carbon nanotubes for the hyperthermia therapy. In particular, despite its good biocompatibility, gold is not a biodegradable material and the injection of Au NPs in vivo can cause their long-term accumulation in the body[9] with unclear consequences. Then, having their absorption/scattering out the window of relative body transparency, Au NPs can hardly provide additional sensing, imaging or therapeutic functionalities as it takes place in cases of more complex gold-based nanostructures such as nanoshells[9] and nanorods[10,11].

Here, we report the effect of strong RF radiation-induced heating of semiconductor silicon (Si) based nanoparticles in aqueous colloidal solutions. Despite much weaker electrical conductivity of Si NPs compared to Au-based counterparts, these NPs manifest similar or better heating rates. We also demonstrate results of successful NPs-based hyperthermia treatment of Lewis lung carcinoma in vivo. We believe that the employment of Si NPs can bring decisive advantages over other inorganic counterparts for cancer treatment tasks. First, Si NPs are not only biocompatible[12], but also biodegradable as in biological tissue they normally decay into orthosilicic acid $Si(OH)_4$, which is naturally excreted from the body through the urine[13]. Second, due to a series of unique properties, including room temperature photoluminescence[12,13], singlet oxygen generation under photoexcitation[14], infrared radiation–induced[15] and ultrasound-induced[16] hyperthermia, Si NPs can offer diagnostic[17,18] and alternative treatment modalities (e.g., Photodynamic Therapy[19,20]) that can be applied in parallel to the RF hyperthermia approach.

In our experiments, we tested two different types of Si-based nanostructures. First, we used NPs produced by mechanical milling of electrochemically-prepared porous silicon (see details in the Methods section). The advantage of the electrochemistry fabrication pathway consists in a fast and cost-efficient production of a large quantity of porous silicon-based (PSi) NPs having promising optical properties[12], although the surface of PSi NPs should be properly cleaned to remove residual contaminants after the fabrication procedure. As shown in Fig. 2a, the electrochemically-prepared PSi NPs have a wide dispersion in size and shape: the size distribution contains a broad spectrum with the peak value at about 50 nm and a considerable portion of larger (several hundreds of nm) NPs. Second, we used Si-based NPs prepared by methods of femtosecond laser ablation in deionized water[21–23] (see details in the Methods section). The latter laser-ablative approach is unique in avoiding any residual contamination of the NP surface as a result of the synthesis in a clean aqueous environment in the absence of any toxic by-products. As shown in Fig. 2b, the laser-ablated Si NPs (LA-Si NPs) have nearly ideal round shape with a much smaller mean size (25–30 nm) and a low size dispersion (less than 15 nm full width at half maximum). Electron diffraction patterns (insets of Fig. 2a,b) show a periodic arrangement of reflections, evidencing the presence of crystalline structure of Si-based NPs. According to the FTIR spectroscopy data (Figure S2 of Suppl. Information (SI)) and XPS data[23], the surface of freshly prepared PSi and LA-Si NPs is predominantly oxidized, with a certain amount of hydrogen still remaining on the PSi NPs surface. Such silicon oxide-related coverage of NPs is supposed to condition hydrophilic properties of their surface. The surface area of PSi NPs was found to be 450 $m^2/g$, while the average pore diameter was about 4 nm (Fig. S1a,b of SI). LA-Si NPs are obviously oxidized due to their interaction with water, although the level of oxidation can be controlled by dosing the amount of dissolved oxygen in deionized water environment during laser synthesis procedure[23]. For comparison, we also used Au NPs prepared by fs laser ablation in deionized water (LA-Au NPs) according to the recipe described in Refs. 21, 22 (see details of the fabrication procedure in the Methods section).

Figure 2 c,d show typical time dependences of the temperature growth of PSi and LA-Si NPs suspensions, as well as of pure deionized water (for comparison), under the exposure in RF radiation with intensity of 5 $W/cm^2$. As shown in the Figure, the heating rate of PSi NPs suspension having the concentration of ~1 mg/mL was about 10 K/min, which was much higher than the heating rate of deionized water (~0.7 K/min). LA-Si NPs were even more efficient RF-radiation sensitizers as they provided a significant heating rate of 5 K/min at 20-fold lower concentration (0.05 mg/mL), while a remarkable heating effect (1.3 K/min) was visible even for ultra-low LA-Si NPs concentrations (0.015 mg/mL) (Fig. 2d). Here, PSi NPs demonstrated a linear growth of solution temperature under the increase of irradiation time, while for LA-Si NPs the temperature growth rate slightly decreased after some irradiation time (~3 min), but still remained reasonably high. The reason of such decrease of the heating rate for LA-Si NPs is not clear and requires further investigation. As one of possibilities, we can imagine a certain modification of surface chemistry or/and size of LA-Si NPs during the RF-induced heating process. For both types of NPs the heating rate was almost linearly dependent on NPs concentration, while LA-Si NPs demonstrated a higher heating rate compared to PSi counterparts for the whole range of NPs concentrations. It should be noted that the reference experiments with aqueous suspension of LA-Au NPs at concentration of ~0.05 $mg/mL$ (Figure S4 of SI) revealed the heating rate ~1.7 $K/min$, which is in agreement with the previously published results[6,7]. Thus, Si NPs suspensions exhibited similar heating rates (or higher in the case of LA-Si NPs) as Au NPs, which are widely

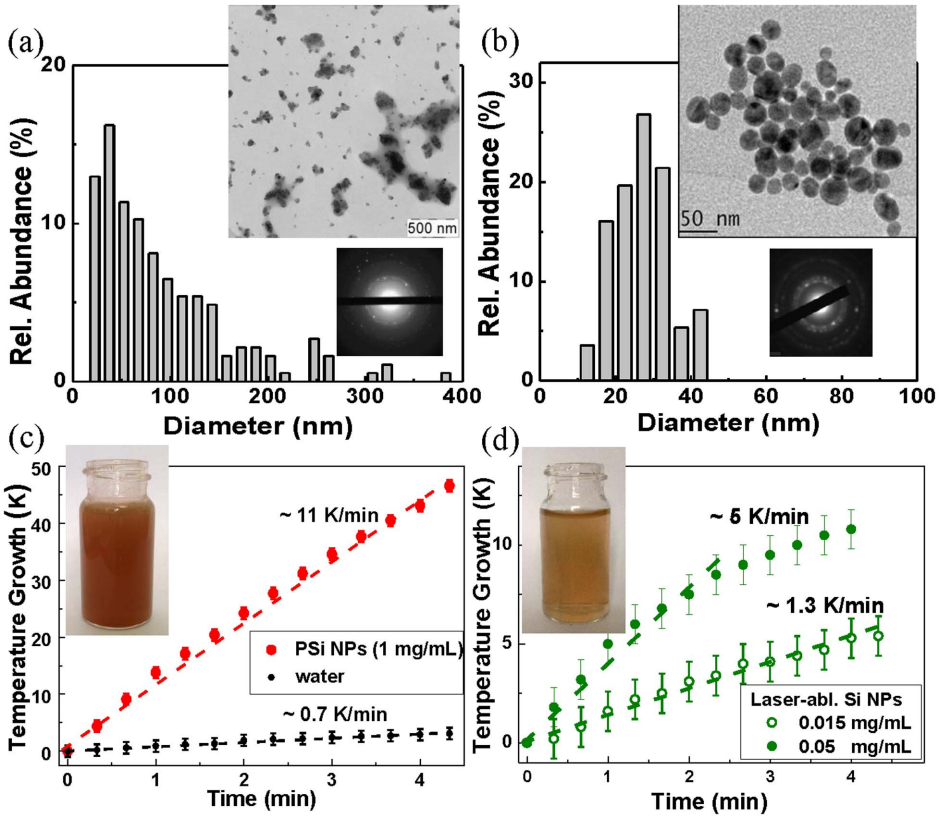


**Figure 2 | Si nanoparticles as nanosensitizers for RF radiation-induced hyperthermia.** (a) TEM image (inset), electron diffraction pattern obtained in the "transmission" geometry (inset) and corresponding size distribution of porous silicon (PSi) nanoparticles prepared by mechanical milling of electrochemically prepared porous silicon; (b) TEM image (inset), electron diffraction pattern (inset) and corresponding size distribution of NPs prepared by laser ablation from a Si target in deionized water; (c) Temperature growth of an aqueous suspension of PSi NPs with concentration of 1 *mg/mL* (red curve) and distilled water (black) under RF irradiation with intensity of 5 $W/cm^2$ versus the RF irradiation time; (d) the same dependence for laser-ablated Si-based NPs with concentration of 0.015 mg/*mL* (open green circles) and 0.05 mg/mL (closed green circles). Insets in panels (c) and (d) show glass cuvettes with the NP suspensions of PSi and LA-Si, respectively.

used for hyperthermia applications. As shown in Figure 3b, the heating rate for 1 mg/mL PSi NPs solution was linearly proportional to RF intensity even if the irradiation time was different (1, 2, 3 minutes).

The heating of NPs solutions can be characterized by considering the Joule's heat dissipation. According to the model proposed by Moran[6], NPs should exhibit sufficient electrical conductivity to efficiently absorb RF radiation. Here, according to an estimation given in Ref. 6, the Joule heating with rate above 10 *K/min* can be achieved in NPs suspensions with concentration of 1 *mg/mL* under RF irradiation with the intensity of 1 $W/cm^2$ if the specific conductivity of NP material is higher than $10^{-1}\ \Omega^{-1}cm^{-1}$. However, this situation is not consistent with our case, as such high conductivity is hardly possible even for Si NPs produced from highly doped crystalline Si wafers[24,25]. Furthermore, our tests did not reveal any remarkable difference between the temperature growth rates for LA-Si NP suspensions produced from undoped and heavily boron-doped Si wafers (Figure S6 of SI). Finally, as shown in Fig. 3a, we did not observe any difference between temperature growth rates for low conductive Si and highly conductive Au NP of similar concentrations (the growth rate of Si NPs was even higher). In fact, it means that either there is an additional mechanism of RF radiation absorption, which is not related to conductivity of NPs material, or the mechanism is not linked to the material conductivity in both cases. The latter supposition is supported by the fact that electrical conductivity of NPs suspensions can depend on surface contaminations and surrounding ions[26] that was not taken into consideration in the above discussed conduction-induced model of the RF heating.

To explain the observed strong heating of weakly conductive Si-based NPs, we propose a novel model of current generation, which is illustrated in Fig. 1b. According to this model, the Joule heating is due to local electrical currents around the NPs rather than to currents over the NPs volume. In the electric field of RF radiation the NP/solution interface is rapidly polarized at the time scale of the order of $10^{-12}$–$10^{-14}$ *sec* and then an electrical double layer surrounding the NPs is formed[27]. In this case, the heating rate $S$ can be estimated by considering the Joule heating in the electrical double layers:

$$S = \frac{N \cdot W}{c \cdot \rho}, \qquad (1)$$

where $N$ is NPs concentration, $W$ is the heat power released per a NP, and $c$ and $\rho$ are the heat capacity and density of water, respectively. Since the RF voltage applied to a NP is proportional to the RF electric field strength and the NP size as $U \sim E \cdot d$ (where $d$ is the diameter of NPs) and the electrical resistivity of the double layer $R$ is also proportional to $d$, the heat power per NP can be derived as:

$$W \sim \frac{U^2}{R} = E^2 d. \qquad (2)$$

For a fixed mass fraction of NPs, concentration of NPs in suspension is determined as $N \sim d^{-3}$. As a result, one can obtain from

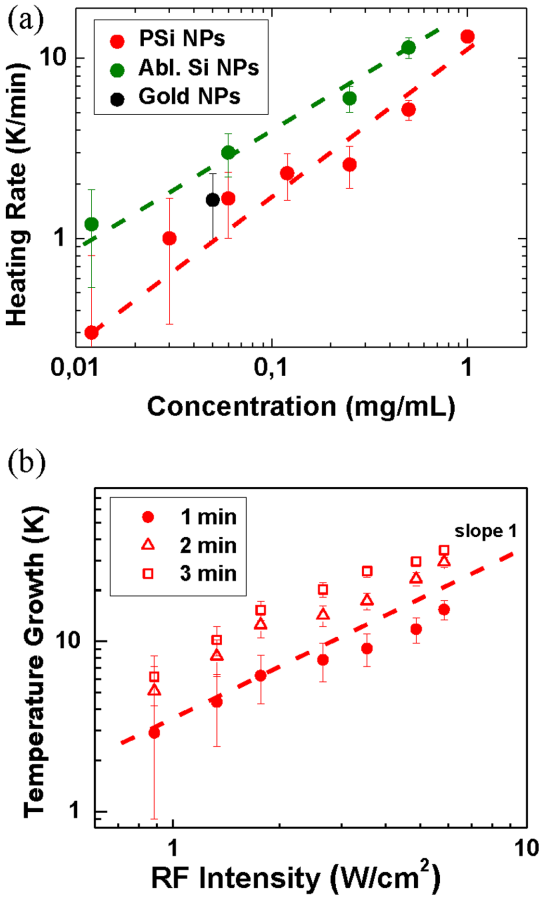


**Figure 3 | Assessment of heating rates in RF radiation-induced hyperthermia using nanosensitizers.** (a) Heating rate of aqueous suspensions of PSi NPs with different concentrations (red circles), LA-Si NPs (green circles) and gold nanoparticles (black circles) under RF exposure at 5 $W/cm^2$. Dashed lines represent linear fits of the experimental data. (b) Temperature increase of an aqueous suspension of PSi NPs with concentration of 1 $mg/mL$ under its RF irradiation for 1 min. (squires), 2 min. (triangles), and 3 min (circles). Dashed line represents a linear fit of the experimental data.

Eq.(1), (2) the following scaling for the heating rate:

$$S \sim 1/d^2 \tag{3}$$

The dependence (3) explains very well the observed lower heating rates (normalized per mass of NPs) for PSi NPs, which are characterized by larger sizes compared to LA-Si-based counterparts (Fig. 3a). It is important that the proposed mechanism is independent of bulk electrical conductivity of NPs that is in good agreement with our experimental data (see Fig. 3a). In principle, this mechanism is somehow valid for highly conductive nanoparticles (Au, Carbon nanotubes) as well, but this situation may require an additional consideration of the Joule heating inside the NP volume.

To assess the potential of Si-based nanomaterials as sensitizers of RF-induced cancer therapy, we first examined the tolerance of PSi and LA-Si NPs for biomedical studies both in vitro and in vivo. The in vitro tests with solutions of both types of NPs of different concentrations did not reveal any toxicity issues that could affect the proliferation of cells (See details in Section 4 of SI). The in vivo tests confirmed our supposition on negligible toxicity of the used nanomaterials. In particular, the examination of the blood content after intragastric in vivo administration of aqueous suspensions of PSi and LA-Si NPs into rats in dosages of 0.7 mg/kg and 4.9 mg/kg did not cause any statistically significant changes in blood levels of aminotrasferases, alkaline phosphatase, bilirubin and cholesterol (see details in Section 6 of SI), which gave evidence for the absence of side effects. Finally, we carried out a series of mice viability tests using intravenous injection of PSi and LA-Si NPs (see details in Section 9 of SI). The NPs were preliminarily covered by dextran to improve NPs transport in the blood stream and minimize immune response. Our experiments showed that the projected therapeutic doses of 10, 20 and 30 mg/kg of PSi and LA-Si NPs did not cause any side effects. This conclusion was made on the basis of analysis of the state and behavior of mice including local reactions and death. Furthermore, for LA-Si NPs we observed a significant increase of mice viability (by 20%) compared to mice from a reference group (see details in Section 9 of SI), although the mechanism of this phenomenon is not yet clear and requires further investigation.

We finally carried out a series of experiments on the assessment of efficiency of RF radiation-induced treatment in biological models. In vitro studies using 3T3 cells revealed high efficiency of PSi and LA-Si sensitizers for RF therapy. The action of RF radiation on the cells, preliminarily loaded with Si NPs, led to drastic cell elimination with the survivor rate not exceeding 12% and 10% for PSi and LA-Si NPs, respectively, whereas the survival rate under the action of RF radiation alone was higher than 90–95% (see details in Section 5 of SI). Finally, carried out *in vivo* tests on the hyperthermia-based treatment of cancer tumors using small animal model (see details in Methods section). 0.5 mL aqueous suspensions of Si-based NPs or equal volumes of sterile water were intratumorally injected and the mice were kept for 15–20 min prior to their RF exposure. Then the mice were immobilized and irradiated with RF for 2 minutes as shown in Fig. 4a. Figure 4b shows a histological image of the tumor performed 1 hour after the injection of Si NPs and Fig. 4c shows the image of tumor at the 3-rd day after the RF-based treatment using PSi NPs as nanosensitizers. One can see that the cancer cells (visible as dark blue spots) experienced a substantial disaggregation after the treatment procedure. Results of the treatment were quantified by the evolution of the total volume occupied by tumor cells. Here, the inhibition of tumor growth was calculated using the following formula:

$$Inhibition = \left(1 - \frac{V}{V_0}\right) \cdot 100\%, \tag{4}$$

where $V$ and $V_0$ are the averaged tumor volumes for the experimental and reference groups of mice, respectively. The positive value of inhibition indicates the inhibition of tumor growth, while the negative one signifies that the average volume for the exposed group of mice is larger than that for the reference group. As shown in Figure 4d, PSi NPs themselves can slightly inhibit the tumor growth. This effect can be explained by the toxic effect of free radicals (dangling bonds) from the surface of Si NPs during the dissolution process. Similar slight inhibition of the tumor growth took place under the action of RF radiation alone (Fig. 4d), which is consistent with previous studies[2–4]. However, our experiments showed that the combined action of PSi NPs and RF excitation could drastically amplify the effect leading to a much stronger inhibition of the tumor growth. Furthermore, as follows from Fig. 4d and Fig. S6 of SI, the efficiency of one time treatment was so high that the average volume of tumor at the 3-rd day after the combined action ($V = 160\ mm^3$) becomes smaller than that volume at the very beginning (day 0) of experiment ($V_0 = 210\ mm^3$). In fact, it means that even without any special optimization of the therapy procedure we achieved a partial elimination of the tumor. As follows from Fig. 4d, laser-ablated NPs provided even more pronounced inhibition of tumor growth after the action of RF radiation (V = 130 $mm^3$) and this effect was observed under much lower number and concentration of NPs (0.2 mL at 0.4 mg/mL compared to 0.5 mL at 1 mg/mL in the case of PSi NPs). Furthermore, we recorded quite different temporal evolution of tumor inhibition after the RF treatment using laser-ablated and

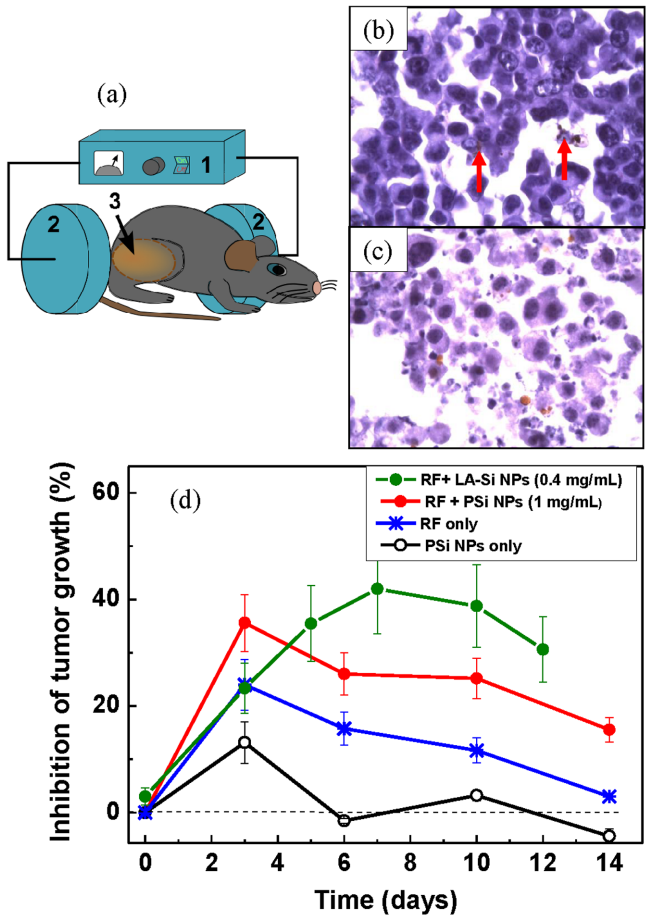


**Figure 4 | *In vivo* assessment of the efficiency of RF radiation-based hyperthermia using Si-based nanosensitizers.** (a) Schematics of the RF radiation-based therapy setup: (1) is a RF radiation source, (2) are the RF electrodes, (3) is a mouse having a tumor area. This Figure was created by the authors; (b) and (c) are histology images of a tumor area 1 h and 3 days after the PSi NP injection and RF-based treatment using PSi NPs as nanosensitizers, respectively. Cancer cells are visible as dark blue spots. Examples of agglomerations of PSi NPs in the cells are indicated by red arrows. (d) Inhibition of the tumor growth after the following treatments: the injection of Si NPs suspension without RF irradiation (black curve); 2 min treatment of tumor area by RF irradiation with the intensity of 2 W/cm$^2$ (blue); injection of a suspension of PSi NPs (0.5 mL, 1 mg/mL) followed by 2 min RF irradiation treatment (red); injection of a suspension of LA-Si NPs (0.2 mL, 0.4 mg/mL) followed by 2 min RF irradiation treatment (green).

PSi NPs sensitizers. Here, the maximal tumor inhibition for LA-Si NPs was observed much later (6–7th days compared to the 3rd day for PSi NPs). These data illustrate a different character of the interaction laser-ablated NPs with biological systems. It should be noted that laser-ablated nanoparticles present an essentially novel object, which is not yet completely studied. Detailed examination of properties of these NPs and their interaction with biological systems will be a subject of our future research. The efficiency of RF radiation-based therapy using PSi and LA-Si sensitizers was confirmed by mice viability tests. Indeed, in average we observed 20–25% increase of mice lifetime after the intratumoral injection of both NPs, followed by RF radiation-based treatment (see details in Section 8 of SI).

The obtained results unambiguously show that Si-based nanoparticles can serve as efficient sensitizers for tasks of RF-induced cancer therapy, resulting not only in the inhibition of the tumor growth, but also in its elimination. We suppose that the observed effect can only be explained by local hyperthermia-based destruction of cancer cells due to the RF-induced heating sensitized by NPs. As shown in Fig. 3a, the efficiency of heating by using Si-based sensitizers appears to be comparable or better than in the case of Au-based NPs. In real cancer treatment procedure, Si-based nanoparticles can be targeted actively, by using proper antibodies, or passively, profiting from the enhanced permeability and retention (EPR) effect consisting in natural capability of NPs to preferably accumulate in tumors[28]. Here, depending on type of tumor and concrete treatment task, one can select nanoparticles with proper characteristics (size, shape, surface oxidation) and additional functionalities (fluorescence etc). Laser-ablated NPs look especially promising for these tasks as they do not contain any residual contaminant on their surface[23,30], exhibit ideal round shape, controlled mean size and low size-dispersion contributing to their better delivery and uptake *in vivo*.

The greatest advantage of Si NPs over other inorganic counterparts consists in their potential biodegradability. Indeed, porous Si-based nanomaterials similar to ones used in our study are known to dissolve in biological environment and excrete from the body through the kidneys and not liver[13], which makes negligible possible side effects (if the surface of NPs is properly cleaned from toxic impurities). Similar biodegradability properties are expected from LA-Si nanoparticles. Such expectation is based on excellent dissolubility of LA-Si NPs in physiological solutions, as follows from our experiments on the control of size of LA-Si NPs by TEM and Raman spectroscopy (see details in Section 2 of SI). Tests in biological environment to confirm the biodegradability of LA-Si NPs are now in progress. Another huge advantage consists in unique optical properties of Si NPs, which promises the involvement of additional imaging or therapeutic modalities. First of all, we can mention prominent fluorescence characteristics of Si-based nanomaterials. Indeed, PSi and other Si-based nanomaterials can exhibit strong fluorescence with quantum yield exceeding 10–15% in the near-IR region of relative tissue transparency (700–900 nm). Furthermore, this fluorescence is characterized by a much longer emission lifetime (5–13 μs) compared to emission signals from organic fluorophores or tissue fluorescence, which makes possible the development of efficient imaging modalities based on time-gated suppression of noises[18]. Finally, both PSi[14] and laser-ablated Si NPs[30] are known to efficiently generate an active form of oxygen (singlet oxygen) under photoexcitation, which promises the employment of photodynamic therapy (PDT) as a parallel cancer treatment channel[19,20]. Similarly, such parallel channel could involve other hyperthermia-based modalities based on heating of Si NPs by IR radiation[15] or ultrasound[16].

In conclusion, we introduced a novel cancer treatment modality using Si nanoparticles as sensitizers of RF radiation-induced hyperthermia. The hyperthermia effect was observed for Si-based nanoparticles produced by both milling of porous silicon and ultraclean laser-ablative growth and was explained by local currents in the electrical double layer near NP surface. In vivo experiments demonstrated that silicon nanoparticles excited by the RF radiation of relatively low intensity not only strongly inhibited the growth of carcinoma tumor, but also led to a decrease of tumor volume. Profiting from potential biodegradability of Si-based nanosensitizers and their prominent optical properties, the proposed RF radiation-based therapy approach looks extremely promising for hyperthermia or/and combined therapy of cancer. Notice that as the main objective of this study we see the demonstration of conceptual possibility for efficient treatment of cancer tumors using Si NPs as RF sensitizers. Next steps imply the optimization of RF-induced NPs heat release and the development of efficient cancer therapy protocols, which should obviously consist of several repetitive RF-based hyperthermia treatment steps using properly optimized parameters of nanoparticles (size, shape, concentration) and RF irradiation doses, in order to achieve a complete elimination of tumors. These studies are now in progress.

## Methods

**Preparation of Si-based nanoparticles by electrochemistry routes.** First, we formed PSi films by electrochemical etching (anodization) of heavily boron-doped crystalline silicon (c-Si) wafers having specific resistivity of 1–10 $m\Omega \cdot cm$ in HF (48%):$C_2H_5OH$ solution (1 : 1) at the current density of 60 $mA/cm^2$ and etching time of 60 $min$. The PSi films were separated from c-Si substrates by applying a pulse of etching current with the current density of 600 $mA/cm^2$. The as-prepared PSi consisted of 5–10 $nm$-sized Si nanocrystals and pores with diameter above 2 nm (mesopores)[29]. The porosity of as-prepared samples was about 70 ± 5%, as determined by gravimetric methods[29]. The porous silicon films were then milled in distilled deionized water by using a planetary mill FRITSCH "Pulverisette 7 premium line" and then centrifuged in an Eppendorf Centrifuge 5424 for 1 min at 2000 rpm. The size of PSi NPs was determined by using a transmission electron microscope (TEM) LEO912 AB OMEGA. The composition of surface coating of PSi NPs was studied with a Fourier-transform infrared (FTIR) spectrometer Bruker IFS 66 v/S. Before measuring FTIR spectra, the suspensions of PSi NPs were deposited on an ATR crystal, dried in air and then evacuated at $10^{-3}$ Torr.

**Preparation of Si- and Au-based nanoparticles by methods of femtosecond laser ablation.** Briefly, a Si or Au target was placed at the bottom of a glass vessel filled with 20 mL of deionized water (18.2 MΩcm). Radiation from Yb:KGW femtosecond laser (Amplitude Systems [Pessac, France], 1025 nm, 480 fs, 500 μJ, 1–5 kHz) was focused with the help of a 750 mm lens onto the target surface to provide the ablation of material[21,22,30]. The target was moved at a scanning velocity of 0.35 mm/s in the focusing plane to obtain identical surface conditions during the laser ablation, while the thickness of the water layer above the target was about 1 cm. Such ablation geometry normally leads to a grey and reddish coloration of the aqueous solution after 2–5 minutes of the experiment with Si and Au, respectively. As the second protocol, we employed methods of two step femtosecond laser fragmentation introduced in a previous study[23]. 10 mL of NPs solution prepared by the first protocol was transferred into a glass cuvette and irradiated, by a focused laser beam of the Yb:KGW femtosecond laser (using the same focusing lens), while the solution was stirred by a magnet to homogenize the ablation process. We used relatively low laser fluence (1 J/$cm^2$) to avoid the phenomenon of laser-assisted plasma breakdown of the liquid, but the radiation intensity was high enough to ablate the suspended nanoparticles.

**Methodology of RF experiments.** The RF heating was produced using a medical apparatus, which is commonly employed for the RF physiotherapy. The apparatus provided RF radiation with frequency of 27 $MHz$ and maximal power up to 66 $W$. The apparatus contained a power source coupled to a pair of flat electrodes with diameter of 38 $mm$ and variable distance between them. The RF electrical field strength between the electrodes was measured by using a metallic antenna connected to an oscilloscope (Agilent 54642A). RF radiation intensity calculated from the electric field strength was in good agreement with the RF power per the electrode surface area. Temperatures of aqueous suspensions of Si NPs and pure water (for comparison) were measured using an infra-red thermometer (AND DT-633) after switching off the RF generator. To investigate the RF heating process a 20 $mL$ glass cuvette was filled with the aqueous suspension of NPs and it was centered between the RF electrodes spaced apart by 42 $mm$, allowing approximately a 6 $mm$ air gap from both sides of the cuvette. The maximum concentration of NPs in suspensions was 1 $mg/mL$, which was estimated using a gravimetrical method. Then, 1 $mg/mL$ suspension was diluted in distilled water to obtain different NPs concentrations. Prior to the RF exposure, the initial temperature of each sample was stabilized in a thermostat at 21°C. The heating rate was quantified by the value of $S = \Delta T/\Delta t$, where $\Delta T$ is temperature increase after the RF exposure for time $\Delta t$.

**Methodology of in vivo tests.** *In vivo* experiments were carried out on lung carcinoma (3LL) tumors inoculated at the left hind paw of male mice of CBA line. The initial tumor volume before the RF treatment was about 210 ± 30 $mm^3$. 0.5 $mL$ aqueous suspensions of PSi or LA-Si NPs or equal volumes of sterile water were intratumorally injected and the mice were kept for 15–20 $min$ prior to RF exposure. Then, the mice were immobilized and irradiated with RF (5 W/$cm^2$) for 2 minutes. A reference group of mice without the RF irradiation was also studied. All experiments on animals were carried out at animal facilities of the Blokhin Cancer Research Centre (Moscow, Russia) in accordance with the Principles of Laboratory Animal Care (NIH publication No. 85–23, revised in 1985) and the European Convention for the Protection of Vertebrate Animals used for Experimental and Other Scientific Purposes (Strasbourg, 18.III.1986, revised by the amending protocol ETS 170). The use of experimental animals was approved by Scientific and Ethic committees of the Blokhin Cancer Research Centre.


1. Custodio, A., Puente, J., Sastre, J. & Diaz-Rubio, E. Second-line therapy for advanced pancreatic cancer: A review of the literature and future directions. *Cancer Treat. Rev.* **35**, 676–84 (2009).
2. Mirza, A. N. *et al.* Radiofrequency ablation of solid tumors. *Cancer J* **7**, 95–102 (2001).
3. Wu, Y. *et al.* High operative risk of cool-tip radiofrequency ablation for unresectable pancreatic head cancer. *J. Surg. Oncol.* **94**, 392–5 (2006).
4. Gannon, C. J. & Curley, S. A. The role of focal liver ablation in the treatment of unresectable primary and secondary malignant liver tumors. *Semin. Radiat. Oncol.* **15**, 265–272 (2005).
5. Gannon, C. J. *et al.* Carbon nanotube-enhanced thermal destruction of cancer cells in a noninvasive radiofrequency field. *Cancer*, **110**, 2654–2665 (2007).
6. Moran, C. H. *et al.* Size-Dependent Joule Heating of Gold Nanoparticles Using Capacitively Coupled Radiofrequency Fields. *Nano Res.* **2**, 400–405 (2009).
7. Cherukuri, P., Glazer, E. S. & Curley, S. A. Targeted hyperthermia using metal nanoparticles. *Adv. Drug Delivery Rev.* **62**, 339–345 (2010).
8. Cardinal, J. *et al.* Noninvasive radiofrequency ablation of cancer targeted by gold nanoparticles. *Surgery* **144**, 125–132 (2008).
9. James, W. D., Hirsch, L. R., West, J. L., O'Neal, P. D. & Payne, J. D. Application of INAA to the build-up and clearance of gold nanoshells in clinical studies in mice. *J. Radioanal. Nucl. Chem.* **271**, 455–459 (2007).
10. Huang, X., El-Sayed, I. H., Qian, W. & El-Sayed, M. A. Cancer cell imaging and photothermal therapy in near-infrared region by using gold nanorods. *J. Am. Chem. Soc.* **128**, 2115–2120 (2006).
11. Kabashin, A. V. *et al.* Plasmonic nanorod metamaterials for biosensing. *Nature Mater.* **8**, 867–871 (2009).
12. Canham, L. T. Bioactive silicon structure fabrication through nanoetching techniques. *Adv. Mater.* **7**, 1033 (1995).
13. Park, J.-H., Gu, L., Maltzahn, G. v., Ruoslahti, E., Bhatia, S. N. *et al.* Biodegradable luminescent porous silicon nanoparticles for in vivo applications. *Nature Mater.* **8**, 331 (2009).
14. Gross, E. *et al.* Spectrally resolved electronic energy transfer from silicon nanocrystals to molecular oxygen mediated by direct electron exchange. *Phys. Rev. B* **68**, 115405 (2003).
15. Lee, C. *et al.* Porous silicon as an agent for cancer thermotherapy based on near-infrared light irradiation. *J. Mater. Chem.* **18**, 4790–4795 (2008).
16. Sviridov, A. P., Andreev, V. G., Ivanova, E. M., Osminkina, L. A., Tamarov, K. P. *et al.* Porous silicon nanoparticles as sensitizers for ultrasonic hyperthermia. *Appl. Phys. Lett.* **103**, 193110 (2013).
17. Osminkina, L. A. *et al.* Photoluminescent biocompatible silicon nanoparticles for cancer theranostic applications. *J. Biophotonics.* **5**, 529 (2012).
18. Gu, L., Hall, D. J., Qin, J., Anglin, E., Joo, J. *et al.* In vivo time-gated fluorescence imaging with biodegradable luminescent porous silicon nanoparticles. *Nature Commun.* **4**, 2336, DOI: 10.1038/ncomms3326 (2013).
19. Timoshenko, V. Yu *et al.* Silicon nanocrystals as photosensitizers of active oxygen for biomedical applications. *JETP Lett.* **83**, 423 (2006).
20. Xiao, L., Gu, L., Howell, S. B. & Sailor, M. J. Porous Silicon Nanoparticle Photosensitizers for Singlet Oxygen and Their Phototoxicity against Cancer Cells. *ACS Nano* **5**, 3651–3659 (2011).
21. Kabashin, A. V. & Meunier, M. Synthesis of colloidal nanoparticles during femtosecond laser ablation of gold in water. *J. Appl. Phys.* **94**, 7941–7943 (2003).
22. Kabashin, A. V. & Meunier, M. Femtosecond laser ablation in aqueous solutions: a novel method to synthesize non-toxic metal colloids with controllable size. *J. Phys.: Conf. Series* **59**, 354–357 (2006).
23. Blandin, P. *et al.* Fs laser fragmentation from water-dispersed microcolloids: toward fast controllable growth of ultrapure Si-based nanomaterials for biological applications. *J. Mater. Chem. B* **1**, 2489–2495 (2013).
24. Theiss, W. Optical properties of porous silicon *Surf. Sci. Rep.* **29**, 191–192 (1997).
25. Timoshenko, V. Yu., Dittrich, Th., Lysenko, V., Lisachenko, M. G. & Koch, F. Free charge carriers in mesoporous silicon. *Phys. Rev. B* **64**, 085314 (2001).
26. Liu, X., Chen, H., Chen, X., Parini, C. & Wen, D. Low frequency heating of gold nanoparticle dispersions for non-invasive thermal therapies. *Nanoscale* **4**, 3945 (2012).
27. Squires, M. T. & Bazant, M. Z. Induced-charge electro-osmosis. *J. Fluid Mech.* **509**, 217–252 (2004).
28. Maeda, H. The Enhanced Permeability and Retention Effect in Tumor Vasculature: The Key Role of Tumor-Selective Macromolecular Drug Targeting. *Adv. Enzyme Regul.* **41**, 189–207 (2001).
29. Herino, R., Bomchil, G., Baria, K., Bertrand, C. & Ginoux, J. L. Porosity and pore-size distributions of porous silicon layers. *J. Electrochem. Soc.* **134**, 1994–2000 (1987).
30. Rioux, D., Laferriere, M., Douplik, A., Shah, D., Lilge, L. *et al.* Silicon Nanoparticles Produced by Femtosecond Laser Ablation in Water as Novel Contamination-Free Photosensitizers. *J. Biomed. Optics* **14**, 021010 (2009).


## Acknowledgments

The authors would like to thank Dr. S. Abramchuk for the TEM measurements, Dr. A. Kudryavtsev and Dr. A. Bychenko for the toxicity tests in vitro and Dr. F. Cheshieva for the blood content test in vivo. Authors acknowledge a financial support of this work by RFBR (project No. 12-02-31266 mol_a), and by Ministry of Education and Science of the Russian Federation (project No. 8737). This work has been carried out thanks to supports of the A*MIDEX project (n° ANR-11-IDEX-0001-02) funded by the «Investissements d'Avenir» French Government program, managed by the French National Research Agency (ANR), LASERNANOBIO project (ANR-10-BLAN_919) of the ANR, and LASERNAN-OCANCER project of the "Plan Cancer" program of INSERM. Porous Si NPs were fabricated by using equipment of the Center of User Facilities of Moscow State University.

## Author contributions

V.N.N., A.V.K. and V.Yu.T. conceived and designed the research. K.P.T., L.A.O., S.V.Z., K.A.M., V.N.N., J.V.K., M.B.G., Y. R., A.A-K. and A.P.S. performed the experiments. K.P.T., L.A.O., S.V.Z., K.A.M., J.V.K., M.B.G., Y.R., A.A-K., A.P.S., M.S., A.V.I., V.N.N., A.V.K. and V.Yu.T. analyzed the data. V.Yu.T. and A.V.K. guided the project. K.P.T., A.V.K. and V.Yu.T. wrote the manuscript with revisions from all authors. All authors have given approval to the final version of the manuscript.

## Additional information

**Supplementary information** accompanies this paper at http://www.nature.com/scientificreports

**Competing financial interests:** The authors declare no competing financial interests.

**How to cite this article:** Tamarov, K.P. *et al*. Radio frequency radiation-induced hyperthermia using Si nanoparticle-based sensitizers for mild cancer therapy. *Sci. Rep.* **4**, 7034; DOI:10.1038/srep07034 (2014).